RNAi screen of the protein kinome identifies checkpoint kinase 1 (CHK1) as a therapeutic target in neuroblastoma

Kristina A. Cole[a,b], Jonathan Huggins[a], Michael Laquaglia[a], Chase E. Hulderman[a], Mike R. Russell[a], Kristopher Bosse[a], Sharon J. Diskin[a], Edward F. Attiyeh[a,b], Rachel Sennett[a], Geoffrey Norris[a], Marci Laudenslager[a], Andrew C. Wood[a], Patrick A. Mayes[a], Jayanti Jagannathan[a], Cynthia Winter[a,b], Yael P. Mosse[a,b], and John M. Maris[a,b,c,1]

[a]Division of Oncology, Children's Hospital of Philadelphia, Philadelphia, PA 19104-4318; [b]Department of Pediatrics, University of Pennsylvania School of Medicine, Philadelphia, PA 19104-4318; and [c]The Abramson Family Cancer Research Institute, University of Pennsylvania School of Medicine, Philadelphia, PA 19104-4318

Edited by Stephen J. Elledge, Harvard Medical School, Boston, MA, and approved December 17, 2010 (received for review August 23, 2010)

Neuroblastoma is a childhood cancer that is often fatal despite intense multimodality therapy. In an effort to identify therapeutic targets for this disease, we performed a comprehensive loss-of-function screen of the protein kinome. Thirty kinases showed significant cellular cytotoxicity when depleted, with loss of the cell cycle checkpoint kinase 1 (CHK1/CHEK1) being the most potent. CHK1 mRNA expression was higher in *MYC–Neuroblastoma-related (MYCN)*–amplified ($P < 0.0001$) and high-risk ($P = 0.03$) tumors. Western blotting revealed that CHK1 was constitutively phosphorylated at the ataxia telangiectasia response kinase target site Ser345 and the autophosphorylation site Ser296 in neuroblastoma cell lines. This pattern was also seen in six of eight high-risk primary tumors but not in control nonneuroblastoma cell lines or in seven of eight low-risk primary tumors. Neuroblastoma cells were sensitive to the two CHK1 inhibitors SB21807 and TCS2312, with median IC_{50} values of 564 nM and 548 nM, respectively. In contrast, the control lines had high micromolar IC_{50} values, indicating a strong correlation between CHK1 phosphorylation and CHK1 inhibitor sensitivity ($P = 0.0004$). Furthermore, cell cycle analysis revealed that CHK1 inhibition in neuroblastoma cells caused apoptosis during S-phase, consistent with its role in replication fork progression. CHK1 inhibitor sensitivity correlated with total MYC(N) protein levels, and inducing MYCN in retinal pigmented epithelial cells resulted in CHK1 phosphorylation, which caused growth inhibition when inhibited. These data show the power of a functional RNAi screen to identify tractable therapeutical targets in neuroblastoma and support CHK1 inhibition strategies in this disease.

Neuroblastoma is an embryonal tumor of early childhood thought to arise from fetal sympathetic neuroblasts (1). Children with localized neuroblastoma can be cured with surgery and/or chemotherapy. About half of children with neuroblastoma have high-risk disease, however, characterized by widespread disease dissemination at diagnosis. For these children, current treatment consists of chemotherapy, surgery, external beam radiation therapy, myeloablative chemotherapy with stem cell rescue, and a maintenance therapy regimen combining retinoids and anti–GD2-based immunotherapy (2). Despite the intense multimodality therapy, at least half of high-risk patients will experience relapse that is almost always fatal and survivors show significant morbidity (1).

To address the unmet need of identifying bona fide molecular targets for drug development in neuroblastoma, we and others have undertaken comprehensive characterization of the neuroblastoma genome, leading to the identification of mutations in the anaplastic lymphoma kinase gene (*ALK*) in 10% of newly diagnosed cases (3, 4). Ongoing comprehensive resequencing efforts will likely discover other potential drug targets in this disease. Although these data may identify the critical genes and pathways for drug development efforts, it is also possible that other key modulators of the malignant phenotype will not show DNA sequence alterations. Thus, we undertook a large-scale loss-of-function screen of the protein kinome with the goal of identifying druggable targets for further therapeutic development in this childhood cancer.

Results

RNAi Kinome Screen Identifies Candidate Therapeutic Targets. To identify kinases involved in neuroblastoma proliferation, we used a loss-of-function approach of depleting 529 kinases individually in four well-characterized neuroblastoma cell lines (SKNAS, EBC1, KELLY, and NLF). Cells were plated overnight and then transfected in triplicate with a pool of four siRNAs targeting each kinase, with positive (siPLK1) and negative controls; they were then screened for inhibition of substrate adherent growth.

To identify the most potent kinases, we developed a prioritization schema outlined in Fig. 1*A*. We ranked the kinases by percentage of relative growth and selected for further study those showing inhibition at less than 0.5 SDs below the mean for the entire set of kinases for each cell line (Dataset S1). This resulted in ~150 kinases per line. Second, we only focused on kinases whose basal expression level was above background on an Illumina gene expression array ($P < 0.05$), resulting in 100 kinases per line. To identify kinases with potentially broad activity, we limited our set to those that showed potent inhibition in at least three of the four cell lines in the screen, resulting in 30 final kinases (Fig. 1 *B* and *C*). These 30 kinases were significantly enriched for proteins involved in cell cycle regulation.

Rediscovery of Kinases Implicated in Neuroblastoma Validated the Screen. Only recently have individual kinases emerged as putative oncogenes in neuroblastoma. Most notably, the *ALK* tyrosine kinase shows heritable germline mutations and is aberrant in ~10% of sporadic cases (3, 4). The KELLY neuroblastoma cell line is the only one in our screen that harbors an *ALK* mutation, and it was therefore reassuring that it emerged as inhibited using our filter thresholds (Fig. 1*B*). The screen also identified inhibition of PLK1, the positive control in our screen, and CDK2, CDK4, and AURKA, each previously implicated in neuroblastoma pathogenesis (5–7), as meeting our thresholds for further investigation.

Author contributions: K.A.C. and J.M.M. designed research; K.A.C., J.H., M. Laquaglia, C.E.H., M.R.R., K.B., R.S., G.N., M. Laudenslager, and A.C.W. performed research; S.J.D., E.F.A., P.A.M., C.W., and Y.P.M. contributed new reagents/analytic tools; K.A.C., J.H., M. Laquaglia, C.E.H., M.R.R., K.B., S.J.D., E.F.A., R.S., M. Laudenslager, A.C.W., P.A.M., J.J., and J.M.M. analyzed data; and K.A.C. wrote the paper.

The authors declare no conflict of interest.

This article is a PNAS Direct Submission.

Data deposition: The data reported in this paper have been deposited in the Gene Expression Omnibus (GEO) database, www.ncbi.nlm.nih.gov/geo (accession no. GSE19274).

[1]To whom correspondence should be addressed. E-mail: maris@chop.edu.

This article contains supporting information online at www.pnas.org/lookup/suppl/doi:10.1073/pnas.1012351108/-/DCSupplemental.

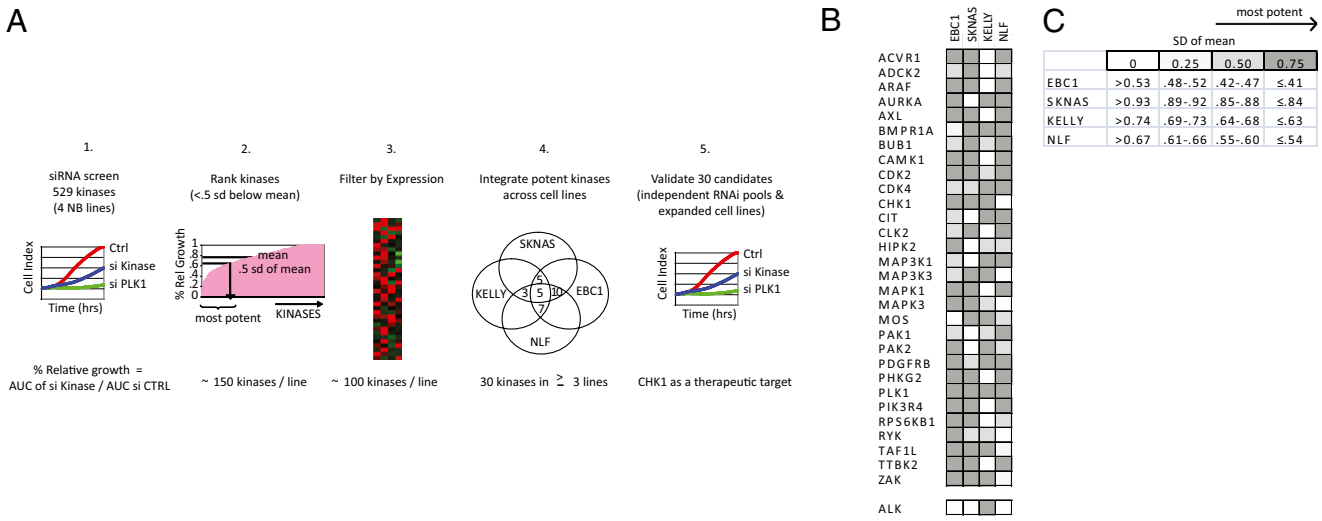

Fig. 1. RNAi screen in neuroblastoma reveals a list of candidate kinase targets. (*A*) Schematic of the RNAi kinase screen in neuroblastoma. (*1*) Four neuroblastoma cell lines were treated with 529 kinase siRNAs and analyzed for substrate adherent growth. (*2*) Most active kinases of each cell line were ranked if the percentage of relative growth (AUC kinase/AUCctrl) was less than 0.5 SD of the mean percentage of relative growth for that line. (*3*) Kinases were further filtered for expression within their line. (*4*) Integration of the most potent kinases. (*B*) Thirty candidate kinases emerged as targets in three or more cell lines in the screen. ALK emerged as a candidate kinase in KELLY, the only *ALK* mutated line in the screen. (*C*) The percentage of relative growth of each cell line was divided by quartile within a cell line and represented as progressively darker boxes by increasing potency.

Loss of Checkpoint Kinase 1 Is Cytotoxic in a Panel of Neuroblastoma Lines. Each of the 30 kinases that met our filtering criteria was validated in the same four cell lines of the initial screen but with an independent set of more specific siRNA pools. The most potent five [checkpoint kinase 1 (CHK1), AURKA, CDK2, CDK4, and MAPK1] were tested in an expanded panel of four additional neuroblastoma cell lines. The most strikingly potent of these was the cell cycle checkpoint protein CHK1, with ≥50% growth inhibition in each neuroblastoma line tested ($n = 8$), including SKNAS, which is typically the most resistant line in our panel (Fig. 2*A*, Fig. S1, and Table 1). Indeed, CHK1 knockdown was cytotoxic by 24 h, reflecting total protein knockdown by this time (Fig. 2 *A* and *B*). Consistent with previous reports that CHK1 depletion does not significantly affect cellular viability in somatic cells in the absence of DNA damaging agents (8–10), the nonneuroblastoma, yet neuronal, immortalized retinal pigmented epithelial (hTERT-RPE1) cells were not inhibited by CHK1 knockdown, despite 98% CHK1 mRNA and protein depletion (Fig. 2 *C–E*).

CHK1 Expression Correlates with MYC–Neuroblastoma-Related Amplification in Neuroblastoma. CHK1 was initially identified in *Schizosaccharomyces pombe* and is evolutionarily conserved (11). It is a serine threonine kinase that regulates the S-phase and G2M checkpoints as well as chromatin remodeling, DNA repair, and replication fork progression in response to replication stress (12). Cancer cells, particularly those with a defective G1 checkpoint, are sensitized to DNA damaging agents with concomitant CHK1 inhibition (13). In contrast, embryonic cells depleted of *CHK1* are not viable, even in the absence of extrinsic DNA damage, and *CHK1*$^{-/-}$ mice die early in embryogenesis (14). In response to DNA damage or stalled replication forks, the ataxia telangiectasia response kinase (ATR) phosphorylates CHK1 on Ser317 and Ser345 (12), and the resulting active CHK1 autophosphorylates at Ser296 (15). Once activated, CHK1 is released from the site of damage to phosphorylate soluble downstream mediators of the DNA damage response pathway. Recently, the MYC and MYC–Neuroblastoma-related (MYCN) oncogenes were reported to have a role in replication independent of their transcriptional activity (16). MYC overexpression caused unscheduled origin firing and replication stress, activating the ATM/ATR-CHK1–dependent DNA damage pathway (16). Therefore, we sought to determine whether there was differential CHK1 expression in *MYCN*-amplified neuroblastoma samples. Analysis of 100 diagnostic primary tumors revealed that CHK1 mRNA is expressed at a significantly higher level ($P < 0.0001$) in *MYCN*-amplified tumors compared with tumors without *MYCN* amplification and in high-risk tumors compared with low-risk tumors ($P = 0.03$) (Fig. 3*A*). Because there is an inverse correlation between *MYCN* amplification and 11q24 hemizygous deletion (where *CHK1* maps) in neuroblastoma, we ensured that the expression difference was not attributable to low CHK1 levels in the *MYCN* single-copy tumors, which would be enriched for samples with an 11q24 deletion (Fig. S2). In a

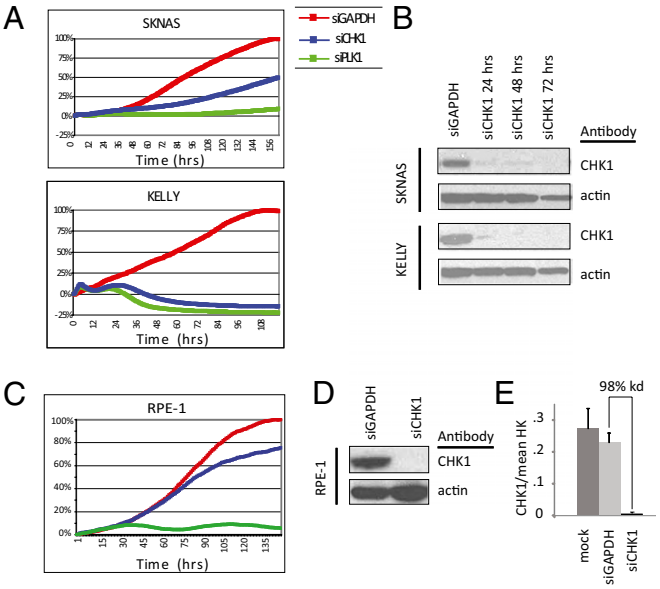

Fig. 2. CHK1 depletion was the most potent inhibitor of neuroblastoma growth. (*A*) Growth curves of neuroblastoma cell lines SKNAS and KELLY treated with siCHK1 and siGAPDH and the positive control siPLK1. (*B*) Western blot of siCHK protein depletion in KELLY and SKNAS. CHK1 depletion does not significantly inhibit the growth of control RPE1 cells (*C*) despite adequate mRNA (*D*) and protein depletion (*E*).

Table 1. Summary of CHK1 inhibition in neuroblastoma cell lines and controls

	MYCN status	TCS (IC_{50}), nM	SB (IC_{50}), nM	CHK1, siRNA	CHK1, S296/actin	MYCN, MYCN/actin	MYC, cMYC/actin
Neuroblastoma lines							
SKNAS*	NA	307	695	0.50	1.17	0.00	0.80
KELLY	AMP	404	676	0.27	2.13	1.90	0.00
NB-EBC1	NA	697	677	0.24	0.42	0.11	0.00
IMR5	AMP	250	459	0.37	1.38	0.61	0.00
CHP134	AMP	973	402	0.40	0.24	1.15	0.00
NB1691	AMP	491	62	0.35	0.54	0.60	0.00
LAN5	AMP	159	161	ND	0.65	1.20	0.00
SKNSH	NA	4,000	4,000	0.26	0.11	0.00	0.46
NLF*	AMP	1,100	1,379	0.11	0.48	0.37	0.00
Nonneuroblastoma lines							
RPE1		2,609	2,356	0.8	0.07	0.00	0.00
MCF7		1,231	2,898	ND	0.09	0.00	0.00
DAOY		517	449	0.35	0.15	0.00	0.67
					P-CHK1	Total MYC	
				Correlation	−0.85	−0.70	
				P value	0.0004	0.0106	

AMP, genomic amplification of *MYCN*; CHK1 siRNA, siRNA inhibition (percentage of relative growth); CHK1, MYCN, and MYC, densitometry of protein band on Western blot/actin band; Correlation, Spearman correlation of the CHK1 Ser-296/Actin or total MYC (MYC + MYCN)/actin bands vs. the corresponding IC_{50}s of TCS; NA, MYCN single copy; ND, not done; SB, IC_{50} of SB; TCS, IC_{50} of TCS.
*p53 mutation.

average, one log higher than in a panel of normal fetal tissues and almost two logs higher than normal adult tissue (Fig. 3*B*).

CHK1 Is Activated in the Absence of Extrinsic DNA Damage in Neuroblastoma. To determine whether the CHK1 protein expressed in neuroblastoma is active, we assayed basal CHK1 phosphorylation in 10 neuroblastoma cell lines. Nine of 10 neuroblastoma cell lines showed detectable phosphorylation of CHK1 at Ser345 and Ser296 (Fig. 3*C*) in the absence of extrinsic DNA damage. The medulloblastoma cell line DAOY, which is a pediatric embryonal brain tumor, also had phosphorylated CHK1. In contrast, control RPE1 and MCF7 (breast cancer) cells did not show detectable levels of phosphorylated CHK1 (Fig. 3*C*), as previously noted for other nonneuroblastoma cell lines (17). None of the other ATR family kinases emerged from our screen because they did not meet our criterion of broad potency. Western blotting of phosphorylated CHK2 (Thr68) in a panel of neuroblastoma cell lines was faint (Fig. S3), and there was no correlation between phospho-CHK2 status and RNAi depletion of CHK2 in two cell lines tested, although CHK2 depletion inhibited KELLY cells (Fig. S3).

As assurance that phosphorylated CHK1 represented neuroblastoma biology and was not a consequence of cell culturing, we analyzed 16 primary diagnostic neuroblastoma tumors. Six of eight samples from high-risk patients showed phosphorylated CHK1 in contrast to only one of eight samples from tumors from children with low-risk disease (Fig. 3*D*). Consistent with the mRNA expression in the primary tumors (Fig. 3*A*), total CHK1 protein levels were high in both the *MYCN*-amplified primary tumors (tumors 260 and 1129) and 2 of the 6 *MYCN* single-copy tumors (Fig. 3*D*); however, accurate levels were likely affected by antibody sensitivity and membrane stripping. DNA sequencing of the 12 coding exons of *CHK1* in five neuroblastoma cell lines sensitive to CHK1 inhibition did not reveal mutations.

Neuroblastoma Cells Are Selectively Sensitive to Pharmacological CHK1 Inhibition. To confirm the cytotoxicity of CHK1 inhibition in neuroblastoma further, and as the next step in translation of our genetic screen, we tested the two small-molecule CHK1 inhibitors SB218078 (SB) and TCS2312 (TCS) in the same panel of neuroblastoma and control cell lines (Fig. 4). Both of these compounds have previously been shown to be chemosensitizers, with single-agent activity only at high micromolar concentrations (18, 19). As shown in Table 1, both compounds decreased the proliferation of neuroblastoma cell lines, with a median IC_{50} value of 564 nM for SB and 548 nM for TCS. Three of the nine dose–response curves are shown for SB in Fig. 4*A*. By 48 h after treatment (500 nM) of either inhibitor, there was complete abrogation of the phospho-Ser296 signal (Fig. 4*B* and Fig. S4). NLF and SKNSH were the only neuroblastoma lines with micromolar IC_{50} values, likely reflecting the low levels of phosphorylated CHK1 (Fig. 3*C*). Both cell lines were sensitive to CHK siRNA depletion, raising the possibility that these cells have developed a resistance to CHK1 inhibition or there are important roles for CHK1 independent of its kinase activity in neuroblastoma tumorigenesis. Control RPE-1 and MCF7 cells also showed IC_{50}s in the micromolar range (Table 1), again likely reflecting the absence of basal CHK1 phosphorylation (Fig. 3*C*). Indeed, by Spearman correlation of CHK1 Ser296 band density and the corresponding IC_{50}s, there was an inverse correlation (−0.85; $P = 0.0004$) between CHK1 Ser296 phosphorylation and the IC_{50} of the CHK1 small-molecule inhibitor TCS (Table 1). Therefore, neuroblastoma cells are selectively sensitive to small-molecule CHK1 kinase inhibitors and there is a correlation between growth inhibition and basal CHK1 Ser296 phosphorylation status.

As the next step in translation of our results, we have begun preclinical testing of PF-00477736, a CHK1 inhibitor that is currently in a phase 1 clinical trial (20). In a pilot study in NB1691 neuroblastoma xenografts, five mice per arm were treated i.p. with vehicle or with 4, 10, or 20 mg/kg of PF-00477736 two times per day. By day 2, there was a dose response to single-agent PF-00477736 treatment (Fig. 4*C*) that was statistically significant compared with controls at 10 mg/kg ($P = 0.03$) and 20 mg/kg ($P = 0.01$). Daily PF-00477736 dosing at 10 mg/kg in NB-1643 xenograft mice revealed a significant decrease in tumor volume compared with vehicle-treated control mice ($P = 0.001$) (Fig. 4*D*). The optimal timing, dosing, and combination studies are underway, but these pilot results suggest that single-agent CHK1 inhibition in neuroblastoma will also be active in vivo.

CHK1 Inhibition in Neuroblastoma Induces Apoptosis During Replication. CHK1 depletion after DNA damage has been shown to cause replication fork collapse (21), mitotic catastrophe (22), and cell cycle arrest (23), depending on the cellular context. Therefore, we sought to determine the mechanisms of growth inhibition after either CHK1 pharmacologic inhibition or siRNA

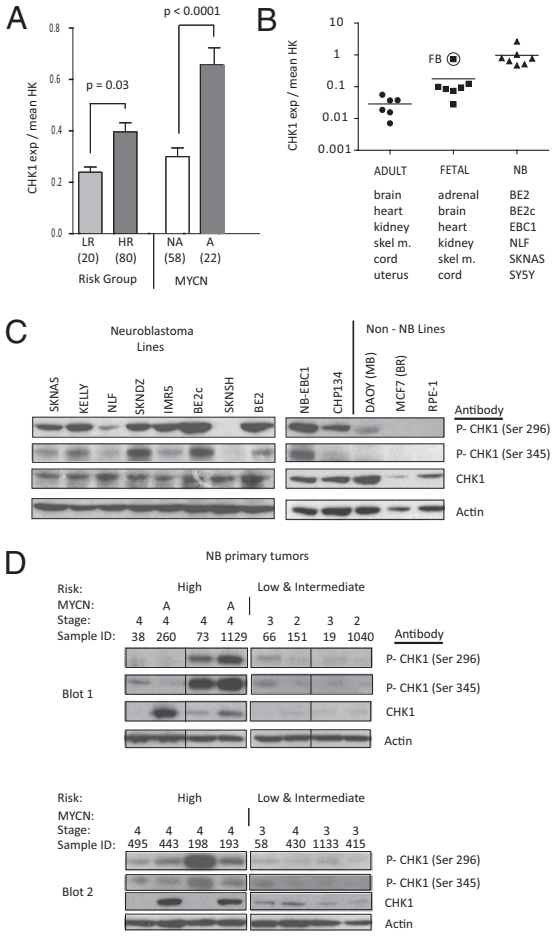

Fig. 3. CHK1 mRNA and protein are highly expressed in neuroblastoma. (*A*) mRNA expression profiling of 100 neuroblastoma diagnostic tumors showed that CHK1 is overexpressed in HR tumors compared with LR tumors (*Left*) and in *MYCN*-amplified tumors compared with *MYCN* NA tumors (*Right*) (mean ± SEM). HR, high-risk; LR, low-risk; NA, single-copy. (*B*) CHK1 mRNA expression by real-time PCR demonstrates that CHK1 is overexpressed in neuroblastoma cell lines and embryonal tissues compared with adult tissues. (*C*) Western blot with constitutive phosphorylation of CHK1 Ser296 and Ser345 in neuroblastoma cell lines compared with control cell lines. (*D*) Western blot of phosphorylation of CHK1 Ser296 and Ser345 and CHK1 in neuroblastoma primary tumors. A, genomic amplification of *MYCN* (samples 260 and 1,129). Each of the two blots (blot 1 and blot 2) had four low/intermediate-risk and four high-risk tumors run in parallel. Fig. S6 shows the original order of blot 1, and blot 2 is ordered as in the figure.

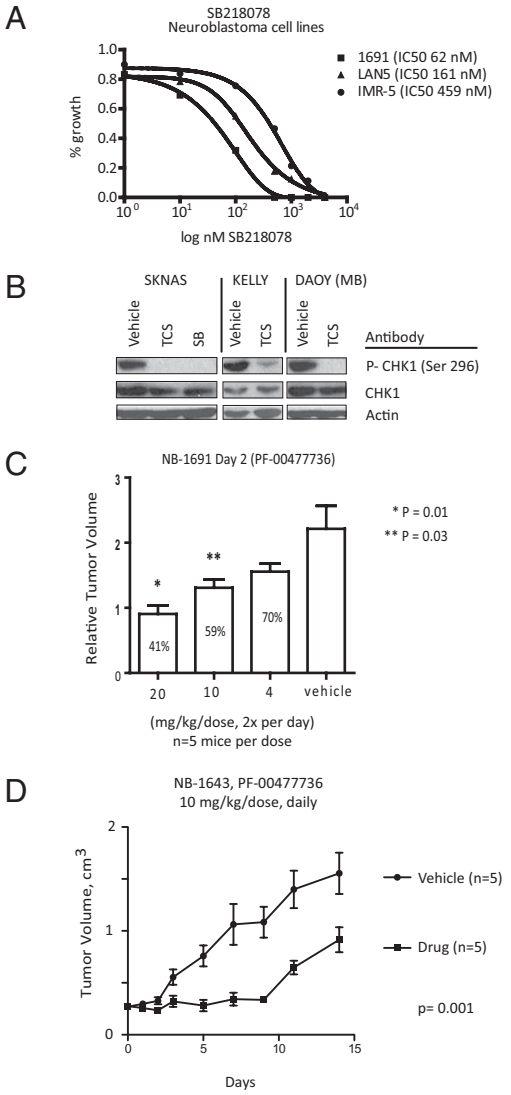

Fig. 4. Pharmacologic inhibition of CHK1 is potent in neuroblastoma cells with activated CHK1. (*A*) Three dose–response curves of SB in neuroblastoma cell lines. (*B*) Western blots of CHK1 Ser296 from KELLY, SKNAS, and DAOY cells treated with 500 nM TCS or SB for 48 h. (*C*) Five mice per cohort bearing NB1691 xenografts are treated with vehicle or with the CHK1 inhibitor PF-00477736 at a dose of 4, 10, or 20 mg/kg twice daily, and relative tumor volumes are determined on day 2 (mean ± SEM). (*D*) Mice bearing NB1643 xenografts are treated daily with 10 mg/kg of the CHK1 inhibitor PF-00477736 for 14 d, and tumor volumes are shown (mean ± SEM).

depletion in neuroblastoma cells. KELLY and SKNAS neuroblastoma cells treated with either inhibitor (500 nM) had a >50% decrease in cellular viability attributable to apoptosis ($P < 0.0001$) (Fig. 5 and Fig. S4). There was no effect on the viability of RPE1 cells by this method (Fig. 5*A*), but there was a sub-G0 population by propidium iodide (PI) staining (Fig. 5*C*). Because CHK1 has a role in the G2M- and S-phase checkpoints, replication, and the mitotic spindle, we sought to determine where in the cell cycle neuroblastoma cells were undergoing apoptosis. Through cell cycle analysis by PI staining of DNA, we found that CHK1 depletion by siRNA (Fig. S4) or pharmacological inhibition (Fig. 5*C* and Fig. S4) caused a significant increase of cells in S-phase compared with controls (68.3 ± 0.6 vs. 36.5 ± 3.2; $P < 0.0001$) consistent with CHK1 depletion in neuroblastoma resulting from a replication defect.

CHK1 Inhibitor Sensitivity Status Correlates with Total MYC Levels. In adult tumor models, cell lines with a p53 mutation are more sensitive to CHK1 inhibition combined with chemotherapy. Although the p53 pathway is intact in most neuroblastoma tumors at diagnosis, up to 50% of relapse tumors acquire a p53 aberration (24). CHK1 inhibitor sensitivity is not predicted by p53 status (Table 1), however. Also, there was no correlation with basal levels of DNA damage as measured by γ-H2Ax protein levels (Fig. S5). Given that neuroblastoma is characterized by aberrant MYC signaling (1, 25), CHK1 is overexpressed in neuroblastoma tumors with *MYCN* amplification (Fig. 3*A*), and MYC overexpression causes replication stress and CHK1 activation (16), we compared total MYC levels (MYCN and MYC) and IC_{50}s in our cell line panel (Fig. S5). Indeed, those cell lines with activated CHK1 had higher levels of total MYC that inversely correlated with inhibitor IC_{50}s (Table 1; Spearman correlation = −0.7; $P = 0.01$).

To support this hypothesis further, we expressed MYCN-ER fusion in RPE1 cells and examined the effect of MYCN in-

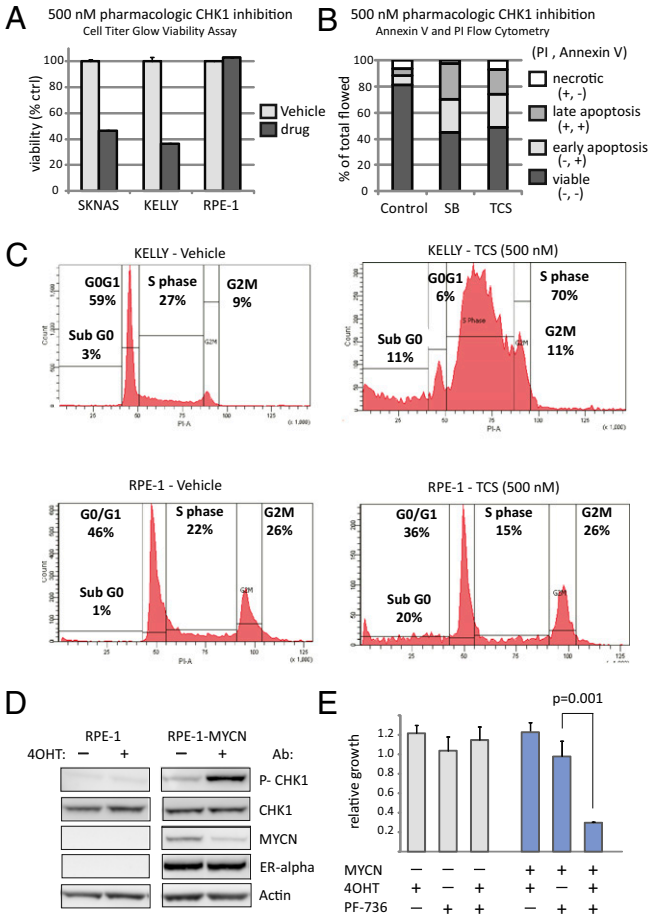

Fig. 5. CHK1 is phosphorylated in response to MYCN activation, and CHK1 inhibition causes apoptosis and replication arrest. (*A*) Treatment of the neuroblastoma cell lines SKNAS and KELLY with the CHK1 inhibitor SB (500 nM) decreased cellular viability by >50% (average ± SD; $P < 0.0001$), whereas the control RPE-1 cells are viable. (*B*) CHK1 inhibition by TCS and SB caused significant apoptosis in KELLY cells by 48 h as determined by annexin/PI staining. (*C*) Representative cell cycle histogram by PI staining demonstrated that CHK1 inhibited by TCS in neuroblastoma KELLY cells harvested at 48 h after treatment are arrested during replication compared with control ($P < 0.0001$), whereas there is no S-phase arrest in RPE1 cells. (*D*) Western blot of CHK1 Ser296, total CHK1, MYCN-ER (as analyzed by an anti-MYCN and an anti-ER antibody, 90 kDa), and actin in RPE1–MYCN-ER or parental RPE1 cells with and without MYCN-ER activation by 4-OHT. (*E*) There is a significant decrease ($P = 0.001$) in cellular growth after CHK1 inhibition by PF-00477736 (PF-736) only in RPE1 cells with activated MYCN (RPE1–MYCN-ER treated with 4-OHT).

duction on CHK1 phosphorylation and cellular proliferation after CHK1 pharmacologic inhibition. As shown in Fig. 5*D*, with the addition of 4-OHT, which activates MYCN by displacing chaperone proteins, allowing MYCN-ER to translocate to the nucleus, CHK1 is phosphorylated in the MYCN-ER cells and not the parental RPE1 cells. We speculate that the MYCN-ER protein decreases because of a negative feedback loop induced by MYCN target genes. MYCN induction does not result in a direct increase in CHK1 protein levels (Fig. 5*D*), although CHK1 mRNA is higher in tumors with MYCN amplification (Fig. 3*A*). CHK1 is not a predicted MYC target (http://www.myc-cancer-gene.org/), suggesting an alternative means of up-regulating mRNA in this patient subset. If MYCN causes replication stress resulting in CHK1 activation, we might expect that RPE1–MYCN-ER cellular growth would be inhibited with CHK1 inhibition, whereas the parental line would not (Fig. 2 and Table 1). Therefore, we treated the RPE1 parental line and RPE1–MYCN-ER cells with and without 4-OHT for 48 h, followed by 500 nM CHK1 inhibitor PF-00477736 or vehicle control and measured substrate adherent growth for 72 h. As shown in Fig. 5*E* (and Fig. S5 for SB), there was a significant decrease in cellular growth in the 4-OHT–activated RPE1–MYCN-ER cells after CHK1 inhibition but not in either the parental RPE1 cells or the MYCN-ER cells treated with PF-00477736 alone.

Discussion

This loss-of-function screen was designed to maximize the likelihood of discovering drug targets that could be translated into a therapy for children with relapsed or refractory neuroblastoma. It was reassuring to rediscover the neuroblastoma oncogene targets ALK and AURKA, both of which have inhibitors that are currently in phase I/II pediatric clinical trials with an expansion cohort for children with neuroblastoma. Although multiple kinases emerged from our screen that could be developed further, the serine threonine kinase CHK1 best met our stringent criteria for a putative drug target with potential broad applicability.

The discovery of CHK1 as a potential therapeutical target for neuroblastoma supports the potential power of an unbiased genetic screen. A priori, CHK1 would not have been a candidate target because: (*i*) its genomic location at 11q24 is one of the most frequent regions of deletion in neuroblastoma; (*ii*) CHK1 has tumor suppressor properties when haploinsufficient (26); and (*iii*) as a single agent, CHK1 inhibition has not been shown to be consistently cytotoxic in any other solid tumor type. Human tumor cell lines in which loss of CHK1 activity has no appreciable effect on proliferation or viability include those derived from carcinomas of the pancreas (27), lung (28), prostate (19), colon (17, 20), or breast (19). In support of our findings, aberrant karyotype AML was recently shown to be sensitive to single-agent CHK1 inhibition, which was synergized with chemotherapy (29). Also, Sidi et al. (30) have reported a previously undescribed mechanism of CHK1-mediated suppression of ionizing radiation-induced apoptosis that is p53-independent, involves ATM and ATR, and causes apoptosis during S-phase when restored through CHK1 depletion.

The precise mechanism of selective sensitivity of CHK1 inhibition in neuroblastoma compared with other human cancers is unknown. Given the greater amount of CHK1 mRNA in *MYCN*-amplified tumors (Fig. 2), correlation between inhibitor sensitivity and total MYC levels (Table 1), and ability of MYCN induction to cause CHK1 phosphorylation (Fig. 5), neuroblastoma's sensitivity to CHK1 inhibition is likely related to oncogenic replicative stress induced by Myc family members. MYC has been recognized to have a very important role in neuroblastoma biology since the discovery of the *MYCN* oncogene more than 20 y ago. Approximately 20% of children with neuroblastoma will have genomic amplification of *MYCN*, conferring such a poor prognosis that they are automatically treated with the most intense therapy available (1). Nevertheless, 60% of children with the most aggressive neuroblastoma do not have *MYCN* amplification. By studying a MYC target gene signature, Fredlund et al. (25) found that MYC pathway activity correlated with high tumor stage and clinical risk group but also predicted clinical outcome in neuroblastoma independent of *MYCN* amplification, including children who otherwise had not previously been recognized as having high-risk disease. Therefore, those cell lines and primary tumors in this study with constitutively phosphorylated CHK1 could have activated myc signaling (or another oncogene) in the absence of *MYCN* amplification.

An alternative hypothesis for the selective sensitivity of neuroblastoma to CHK1 inhibition is that it is synthetic lethal for an alternative pathway involved in the damage response or repair network. For example, Chen et al. (31) reported that cell lines depleted of the Fanconi anemia genes are sensitive to single agent CHK1 inhibition but not their isogenic complemented lines. Although mutations in the DNA damage response genes have not been reported in neuroblastoma to date, we recently found a significant genome-wide association signal within the *BARD1* (*BRCA1* Ring Domain 1) gene suggesting that the DNA damage response pathway may have an important role in neuroblastoma tumorigenesis (32).

CHK1 inhibitors have been in clinical trials for over a decade (33). More specific CHK1 inhibitors are in currently in development in adult phase 1/2 clinical trials in combination with chemotherapy and radiation (20, 33). In summary, we have identified CHK1 as a therapeutic target for neuroblastoma that may provide an additional therapy option for children with high-risk, refractory, or relapsed disease.

Materials and Methods

siRNA Transfection. The Thermo Scientific kinase siGenome library included a set of 529 kinase pools containing four different siRNAs. The siRNA transfection and analysis were performed as previously described (3). For the validation and siCHK experiments, Thermo Scientific ON-Target Plus siRNAs were used (Table S1). In brief, 0.8–1 $\times$ 10^4 neuroblastoma cells were plated overnight in 96-well plates on the xCELLigence system (F. Hoffman-La Roche), transfected in triplicate, and monitored continuously for 100 h. The area under the curve was calculated for each siRNA triplicate and mock transfection. The percentage of relative growth was measured by the following formula (% relative growth = AUC siKinase/AUC siControl).

Pharmacological Inhibition. The CHK1 inhibitors SB and TCS were purchased from Tocris Bioscience. Twenty-four hours after plating, cells were treated in triplicate with eight increasing concentrations of drug (range: 1–4,000 nM) and a DMSO control. Cellular growth was monitored on the xCELLigence System. At 72 h after treatment, the IC_{50} was determined with a five-parametric linear mixed-effects model (Prism; Graphpad).

In Vivo Studies. CB17SC-M *scid*$^{-/-}$ mice were used to propagate s.c. implanted neuroblastoma tumors. Caliper measurements were obtained, and tumor volumes were calculated using the formula, $(\pi/6) \times d^2$, where d represents the mean diameter. Mice bearing NB-1691 tumors were randomized (n = 5 per arm) to treatment with 4, 10, or 20 mg/kg of PF-00477736 (Pfizer, Inc.) or vehicle administered i.p. twice daily when tumors were 100–200 mm^3. Mice bearing NB-1643 tumors were randomized (n = 5 per arm) once the tumor was greater than 200 mm^3 to treatment with 10 mg/kg of PF-00477736 or vehicle control administered i.p. daily for 15 d. All animal studies were approved by the Children's Hospital of Philadelphia Institutional Animal Care and Use Committee.

Flow Cytometry. Cultured cells (30×10^5) were transfected either with 50 nM CHK1 and *GAPDH* siRNAs or with 500 nM TCS, SB, or vehicle in six-well plates in duplicate. After 48 h, media and cells were gently harvested and analysis of apoptosis was determined by Annexin V/PI staining or fixed and stained by PI for cell cycle analysis (34). Independent experiments were performed a minimum of three times.

Viability Assay. Cells (1×10^4 per well) were treated in triplicate with 500 nM SB, TCS, or vehicle in a 96-well plate, and cellular viability was determined with a CellTiter-Glo (Promega).

CHK1 Phosphorylation and Inhibition in RPE1–MYCN-ER Cells. The immortalized MYCN-ER–hTERT RPE1 cell line was kindly provided by Michael Hogarty (Children's Hospital of Philadelphia, Philadelphia, PA). RPE1–MYCN-ER and parental RPE1 cells were plated overnight and treated with 400 nM 4-OHT or vehicle, and lysates were harvested at 24 h. Western blots for CHK1 Ser296, total CHK1, MYCN, ER-α, and actin were performed. For pharmacologic CHK1 inhibition experiments, 2,500 RPE1–MYCN-ER and parental RPE1 cells were plated overnight in triplicate on the xCELLigence system and treated with and without 400 nM 4-OHT for 48 h, followed by 500 nM CHK1 inhibitor PF-00477736 (or SB), vehicle control, or no treatment, and growth was determined as above. Three independent experiments were performed.

Statistical Analysis. Group comparisons were determined with a two-sided t test and Spearman correlation testing using Graphpad Prism; a P value <0.05 was considered as significant. For the longitudinal xenograft experiment, a linear mixed-effects model was used to test the difference in the rate of tumor volume change over time between the treatment and vehicle groups.

For additional details on cell culture, gene expression profiling, real-time RT-PCR, immunoblotting, and DNA sequencing, see *SI Materials and Methods*.

ACKNOWLEDGMENTS. We thank Dr. Michelle Garrett from the Institute of Cancer Research and Dr. Craig Basing from the University of Pennsylvania for helpful discussions and advice. We also acknowledge the Children's Oncology Group (Grant U10-CA98543) for providing blood and tumor specimens from patients with neuroblastoma. This work was supported, in part, by the Super-Jake Foundation (J.M.M. and K.A.C.), the Children's Neuroblastoma Cancer Foundation (K.A.C.), National Institutes of Health Grants K08 CA136979-01 (to K.A.C.) and R01-CA87847 (to J.M.M.), the Alex's Lemonade Stand Foundation (J.M.M.), and the Abramson Family Cancer Research Institute (J.M.M.).

1. Maris JM (2010) Recent advances in neuroblastoma. *N Engl J Med* 362:2202–2211.
2. Matthay KK, et al. (1995) Role of myeloablative therapy in improved outcome for high risk neuroblastoma: Review of recent Children's Cancer Group results. *Eur J Cancer* 31A: 572–575.
3. Mossé YP, et al. (2008) Identification of ALK as a major familial neuroblastoma predisposition gene. *Nature* 455:930–935.
4. George RE, et al. (2008) Activating mutations in ALK provide a therapeutic target in neuroblastoma. *Nature* 455:975–978.
5. Molenaar JJ, et al. (2009) Inactivation of CDK2 is synthetically lethal to MYCN over-expressing cancer cells. *Proc Natl Acad Sci USA* 106:12968–12973.
6. Molenaar JJ, et al. (2008) Cyclin D1 and CDK4 activity contribute to the undifferentiated phenotype in neuroblastoma. *Cancer Res* 68:2599–2609.
7. Otto T, et al. (2009) Stabilization of N-Myc is a critical function of Aurora A in human neuroblastoma. *Cancer Cell* 15:67–78.
8. Chen Z, et al. (2003) Human Chk1 expression is dispensable for somatic cell death and critical for sustaining G2 DNA damage checkpoint. *Mol Cancer Ther* 2:543–548.
9. Petermann E, Caldecott KW (2006) Evidence that the ATR/Chk1 pathway maintains normal replication fork progression during unperturbed S phase. *Cell Cycle* 5:2203–2209.
10. Toledo LI, Murga M, Gutierrez-Martinez P, Soria R, Fernandez-Capetillo O (2008) ATR signaling can drive cells into senescence in the absence of DNA breaks. *Genes Dev* 22: 297–302.
11. Sanchez Y, et al. (1997) Conservation of the Chk1 checkpoint pathway in mammals: Linkage of DNA damage to Cdk regulation through Cdc25. *Science* 277:1497–1501.
12. Zhou BB, Bartek J (2004) Targeting the checkpoint kinases: Chemosensitization versus chemoprotection. *Nat Rev Cancer* 4:216–225.
13. Bucher N, Britten CD (2008) G2 checkpoint abrogation and checkpoint kinase-1 targeting in the treatment of cancer. *Br J Cancer* 98:523–528.
14. Takai H, et al. (2000) Aberrant cell cycle checkpoint function and early embryonic death in Chk1(–/–) mice. *Genes Dev* 14:1439–1447.
15. Clarke CA, Clarke PR (2005) DNA-dependent phosphorylation of Chk1 and Claspin in a human cell-free system. *Biochem J* 388:705–712.
16. Dominguez-Sola D, et al. (2007) Non-transcriptional control of DNA replication by c-Myc. *Nature* 448:445–451.
17. Walton MI, et al. (2010) The preclinical pharmacology and therapeutic activity of the novel CHK1 inhibitor SAR-020106. *Mol Cancer Ther* 9:89–100.
18. Jackson JR, et al. (2000) An indolocarbazole inhibitor of human checkpoint kinase (Chk1) abrogates cell cycle arrest caused by DNA damage. *Cancer Res* 60:566–572.
19. Teng M, et al. (2007) Structure-based design and synthesis of (5-arylamino-2H-pyrazol-3-yl)-biphenyl-2′,4′-diols as novel and potent human CHK1 inhibitors. *J Med Chem* 50:5253–5256.
20. Zhang C, et al. (2009) PF-00477736 mediates checkpoint kinase 1 signaling pathway and potentiates docetaxel-induced efficacy in xenografts. *Clin Cancer Res* 15:4630–4640.
21. Paulsen RD, Cimprich KA (2007) The ATR pathway: Fine-tuning the fork. *DNA Repair (Amst)* 6:953–966.
22. Huang X, Tran T, Zhang L, Hatcher R, Zhang P (2005) DNA damage-induced mitotic catastrophe is mediated by the Chk1-dependent mitotic exit DNA damage checkpoint. *Proc Natl Acad Sci USA* 102:1065–1070.
23. Wilsker D, Petermann E, Helleday T, Bunz F (2008) Essential function of Chk1 can be uncoupled from DNA damage checkpoint and replication control. *Proc Natl Acad Sci USA* 105:20752–20757.
24. Carr-Wilkinson J, et al. (2010) High Frequency of p53/MDM2/p14ARF Pathway Abnormalities in Relapsed Neuroblastoma. *Clin Cancer Res* 16:1108–1118.
25. Fredlund E, Ringnér M, Maris JM, Påhlman S (2008) High Myc pathway activity and low stage of neuronal differentiation associate with poor outcome in neuroblastoma. *Proc Natl Acad Sci USA* 105:14094–14099.
26. Lam MH, Liu Q, Elledge SJ, Rosen JM (2004) Chk1 is haploinsufficient for multiple functions critical to tumor suppression. *Cancer Cell* 6:45–59.
27. Azorsa DO, et al. (2009) Synthetic lethal RNAi screening identifies sensitizing targets for gemcitabine therapy in pancreatic cancer. *J Transl Med* 7:43.
28. Zabludoff SD, et al. (2008) AZD7762, a novel checkpoint kinase inhibitor, drives checkpoint abrogation and potentiates DNA-targeted therapies. *Mol Cancer Ther* 7:2955–2966.
29. Cavelier C, et al. (2009) Constitutive activation of the DNA damage signaling pathway in acute myeloid leukemia with complex karyotype: Potential importance for checkpoint targeting therapy. *Cancer Res* 69:8652–8661.
30. Sidi S, et al. (2008) Chk1 suppresses a caspase-2 apoptotic response to DNA damage that bypasses p53, Bcl-2, and caspase-3. *Cell* 133:864–877.
31. Chen CC, Kennedy RD, Sidi S, Look AT, D'Andrea A (2009) CHK1 inhibition as a strategy for targeting Fanconi Anemia (FA) DNA repair pathway deficient tumors. *Mol Cancer* 8:24.
32. Capasso M, et al. (2009) Common variations in BARD1 influence susceptibility to high-risk neuroblastoma. *Nat Genet* 41:718–723.
33. Dai Y, Grant S (2010) New insights into checkpoint kinase 1 in the DNA damage response signaling network. *Clin Cancer Res* 16:376–383.
34. Cole KA, et al. (2008) A functional screen identifies miR-34a as a candidate neuroblastoma tumor suppressor gene. *Mol Cancer Res* 6:735–742.